Supporting Information for

Influence of the TiO_2 Electronic Structure and of Strong Metal-Support Interaction on Plasmonic Au Photocatalytic Oxidations

A. Naldoni, [a] F. Riboni,[b,‡] M. Marelli, [a] F. Bossola,[c] G. Ulisse,[d] A. di Carlo,[d] I. Pïs,[#,f] S. Nappini,[f] M. Malvestuto,[e] M. V. Dozzi, [b] R. Psaro, [a] E. Selli,*[,b] and V. Dal Santo.*[,a]

[a] CNR-Istituto di Scienze e Tecnologie Molecolari, Via Golgi 19, 20133 Milan, Italy
[b] Dipartimento di Chimica, Università degli Studi di Milano, Via Golgi 19, 20133 Milan, Italy.
[c] Dipartimento di Scienza e Alte Tecnologie, Università dell'Insubria, 22100 Como, Italy
[d] University of Rome "Tor Vergata", Department of Electronic Engineering, Via del Politecnico 1, 00133 Rome, Italy
[e] Elettra-Sincrotrone Trieste S.C.p.A., S.S. 14 Km 163.5, AREA Science Park - Basovizza, 34149 Trieste, Italy
[f] IOM CNR, Laboratorio TASC, S.S. 14 Km 163.5, AREA Science Park – Basovizza, 34149 Trieste, Italy
‡ *current address*: Department of Materials Science WW4-LKO, University of Erlangen-Nuremberg, Martenstrasse 7, 91058, Erlangen, Germany

Index

Figures 2

Tables 8

Evaluation of heat generated by the Au LSPR excitation 10

Figures

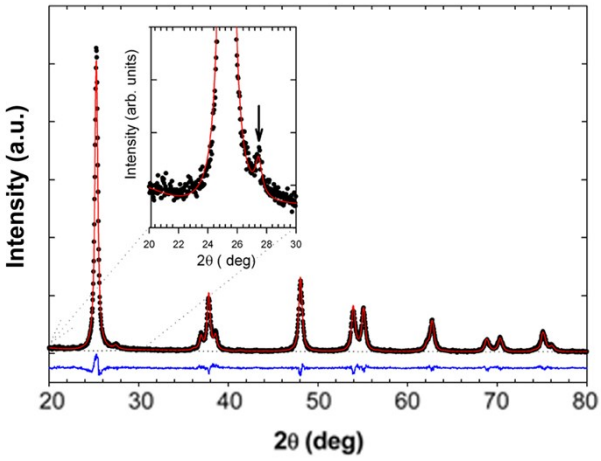

Figure S1. XRPD pattern of N-TiO_2 acquired for long time; the inset represents the zoom of the 2θ-region where the rutile contribution is clearly visible (peak indicated by the arrow).

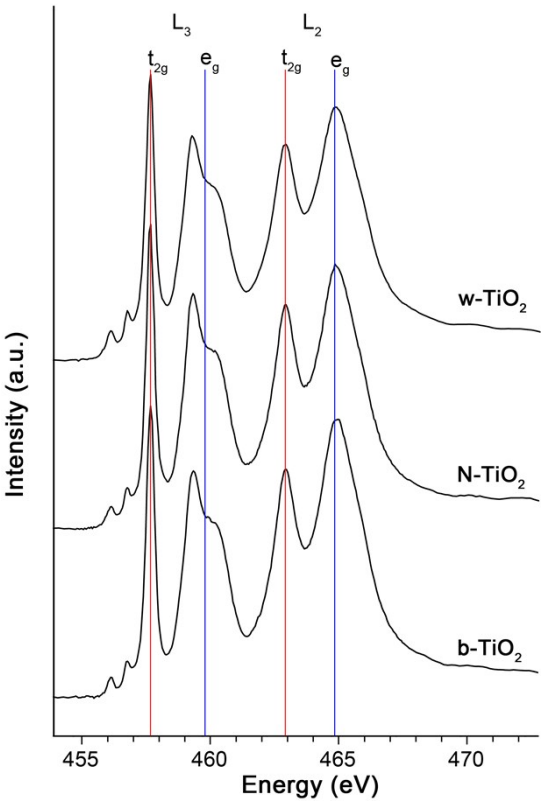

Figure S2. XAS spectra at the Ti $L_{2,3}$ edge of w-TiO_2, N-TiO_2 and b-TiO_2.

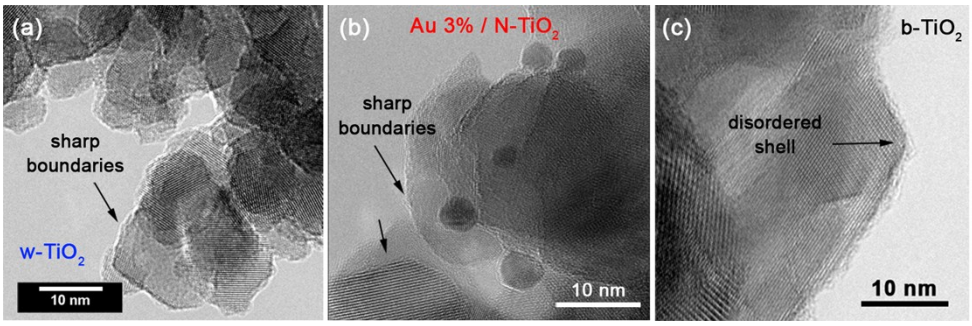

Figure S3. HRTEM micrograph showing the nanocrystal boundary features for (a) w-TiO_2, (b) N-TiO_2, and (c) b-TiO_2.We report representative TEM images that show the Au/TiO_2 interface formed after the Au NPs deposition for Au 3%/N-TiO_2.

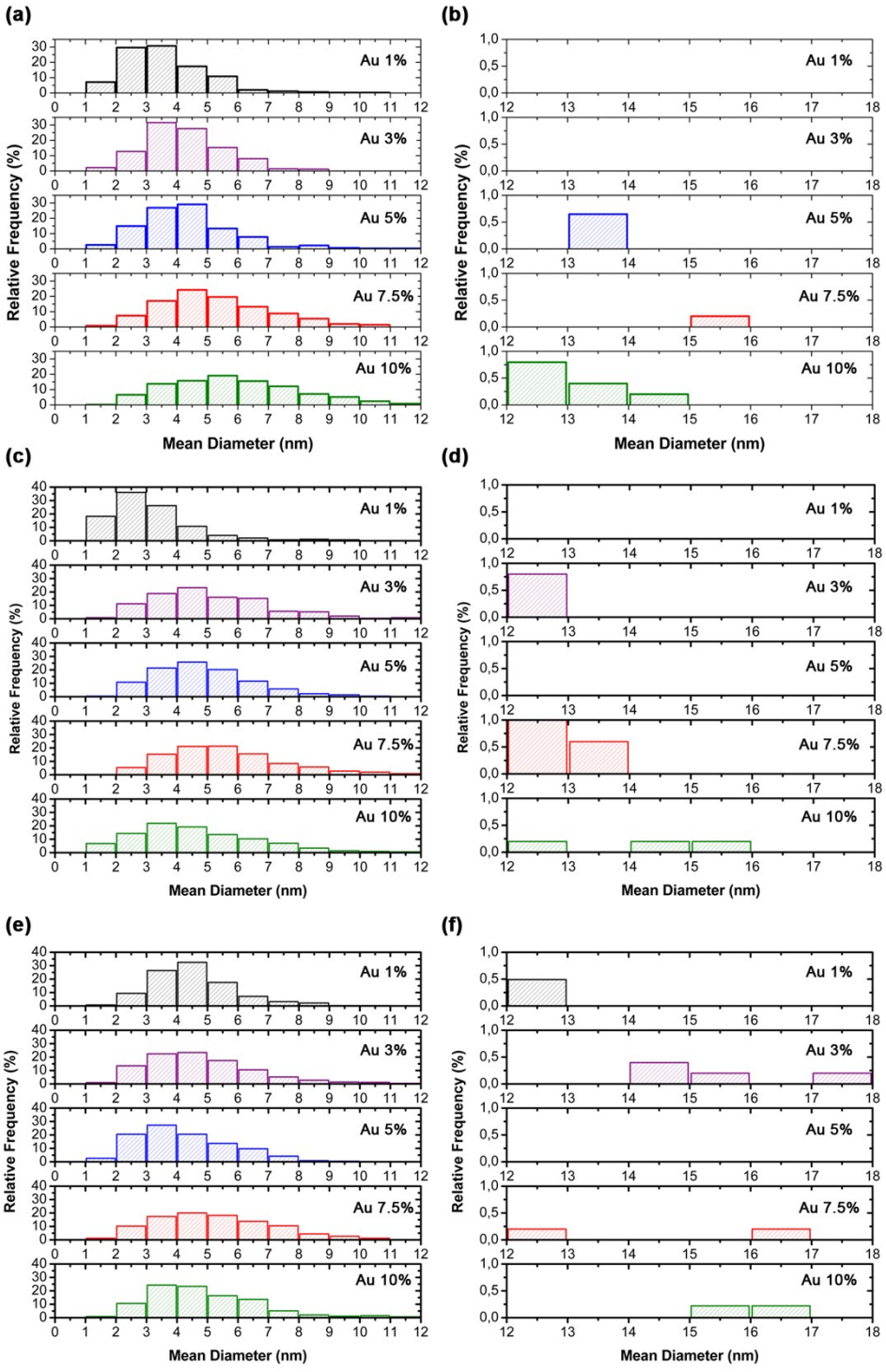

Figure S4. Size distribution obtained from the analysis of TEM images of gold nanoparticles deposited on (a,b) w-TiO_2, (c,d) b-TiO_2, (e,f) N-TiO_2. The size distribution was divided into two dimensional regimes: (a,c,e) represent the 1-12 nm region, while (b,d,f) show the 12-18 nm range for the Au modified w-, b- and N-TiO_2 series.

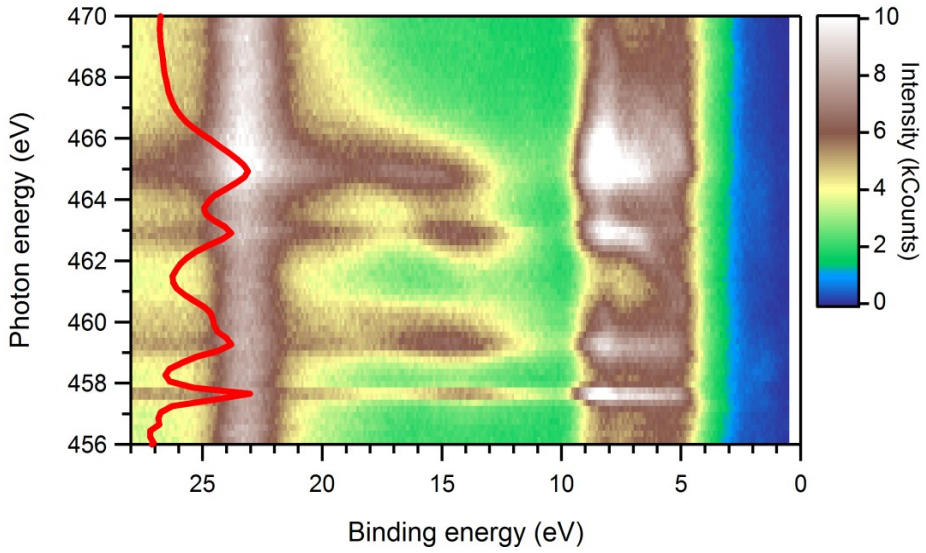

Figure S5. Contour plot of the normalized RESPES data, along with the Ti *2p–3d* X-ray absorption spectrum (left axis) for w-TiO_2.

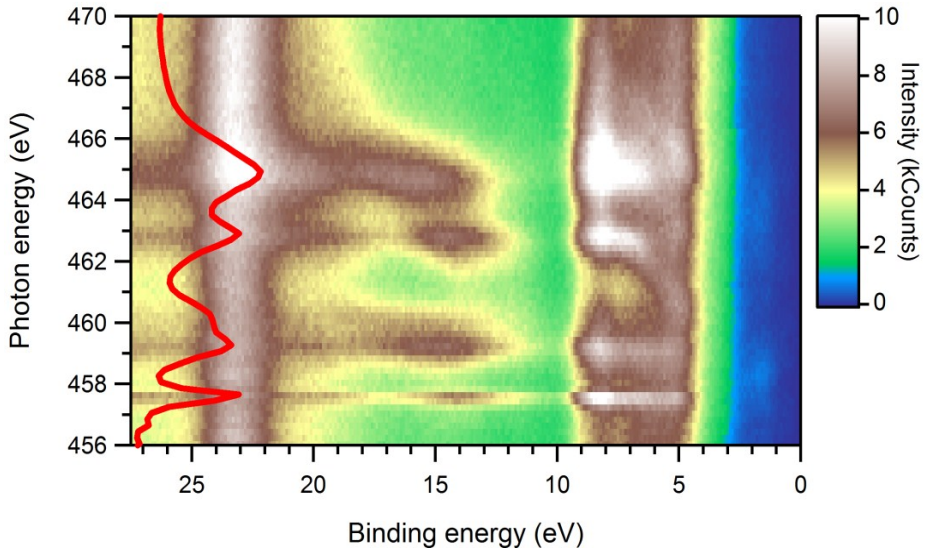

Figure S6. Contour plot of the normalized RESPES data, along with the Ti *2p–3d* X-ray absorption spectrum (left axis) for N-TiO_2.

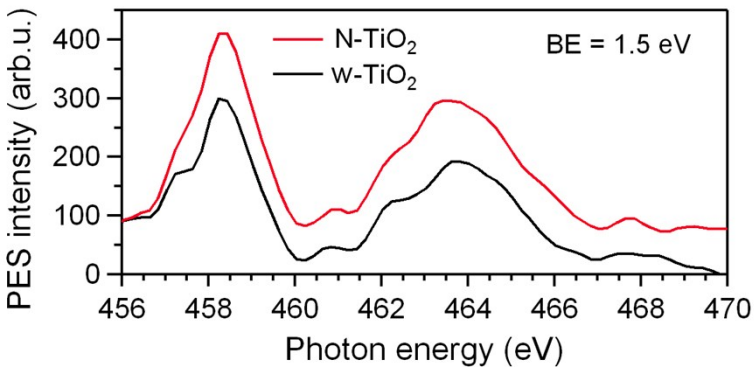

Figure S7. Photoemission spectra (PES) at the maximum of intragap states levels (Binding Energy = 1.5 eV) for w-TiO_2 (black curve) and N-TiO_2 (red curve).

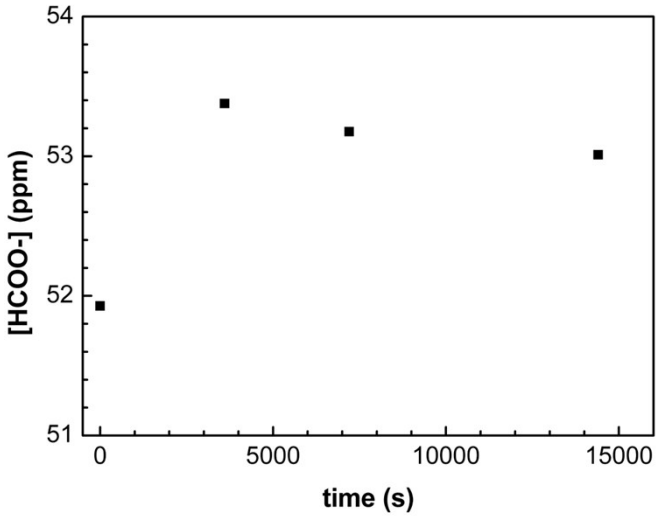

Figure S8. Photocatalytic run of FA degradation performed with bare N-TiO_2.

All the unmodified titania samples (*i.e.*, w-, N- and b-TiO_2 with no Au NPs) exhibited no photoactivity toward FA oxidation (see the representative results for N-TiO_2 in Figure S9(a)), owing to the relatively large band gap of TiO_2 which, notoriously, cannot be excited with visible light (E_g = *ca.* 3.2 eV and λ_{edge} = *ca.* 380 nm). These results were a preliminary confirmation that FA photodegradation under green LED irradiation (λ = 532 nm) is promoted by a mechanism activated by the LSPR of Au NPs.

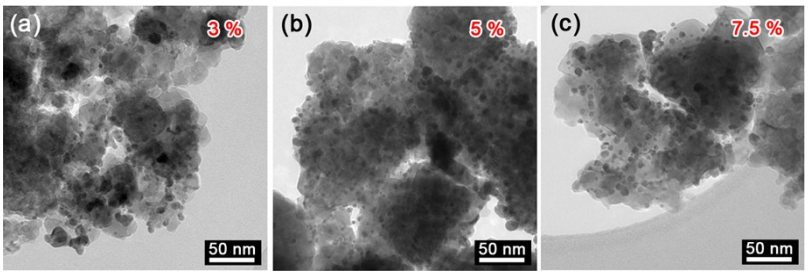

Figure S9.TEM images showing the increased Au NPs density from 3% to 7.5 % Au/N-TiO_2 samples.

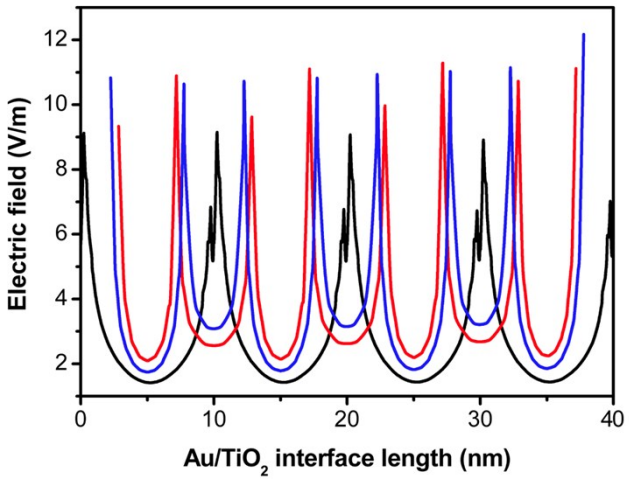

Figure S10. Electric field generated by Au nanoparticles LSPR on the TiO_2 surface. The electric field is strongly enhanced in the point where Au NPs are in contact with TiO_2. In particular, when SMSI = 0 nm (black line), one hot spot forms at the Au/TiO_2 contact point; differently, when SMSI = 1 (red line) and 2 nm (blue line) the profile lines present two hot spots, corresponding to the two-contact Au/TiO_2 interface.

Tables

Table S1. Phase composition (A = anatase, R = rutile) and anatase nanoparticle dimensions, d_A, obtained from XRD analysis.

	Phase composition (wt.%)	**d_A (nm)**
w-TiO_2	100 A	16
N-TiO_2	98 A / 2 R	22
b-TiO_2	81 A / 19 R	23

Table S2. Real gold content (wt.%) of all investigated photocatalysts, as determined through ICP-OES, Au nanoparticles mean diameter, d_{Au}, obtained from HRTEM analysis, and specific surface area (SSA) for all investigated samples.

	w-TiO_2			**N-TiO_2**			**b-TiO_2**		
Au (wt.%)	**ICP (wt.%)**	**d_{Au} ± SE (nm)**	**SSA (m^2 g^{-1})**	**ICP (wt.%)**	**d_{Au} ± SE (nm)**	**SSA (m^2 g^{-1})**	**ICP (wt.%)**	**d_{Au} ± SE (nm)**	**SSA (m^2 g^{-1})**
1	0.70	3.6±0.07	79	0.76	3.2±0.07	21	0.83	4.6±0.07	3.2
3	2.31	4.3±0.06	69	2.69	5.2±0.09	21	2.89	4.9±0.13	4.5
5	4.00	4.4±0.10	79	4.44	4.8±0.07	18	4.48	4.2±0.07	3.3
7.5	6.24	5.3±0.08	65	6.92	5.7±0.09	19	8.66	5.3±0.09	1.2
10	8.90	5.9±0.10	81	8.69	4.7±0.09	16	9.32	4.9±0.10	3.0

Table S3. Refractive index (n) and extinction coefficient (k) values of the materials simulated by means of the Finite Difference Time Domain method. (data taken from: P.-G.Wu, C.-H. Ma, J. K. Shang, Appl. Phys. A 2005, 81, 1411–1417)

Material	n	k
w-TiO_2	2.5586	4.04e-4
N-TiO_2	2.400	4.04e-4
H_2O	1.334	1.32e-9
Au nanoparticle	0.432	2.437

Table S4. Enhancement Factor (EF %) of the electric field calculated simulating 6 nm-sized Au NPs, with interparticles distance 2 nm < d_{Au-Au} < 10 nm (Δd_{Au-Au} = 1 nm) and different extents of metal nanoparticles embedding in the w-TiO_2 and N-TiO_2 supports (*i.e.*, SMSI = 0, 1 and 2 nm). A graphical representation of the data is provided in Figure 8.

	Enhancement Factor (EF %)					
	w-TiO_2			**N-TiO_2**		
d_{Au-Au} (nm)	**SMSI = 0 nm**	**SMSI = 1 nm**	**SMSI = 2 nm**	**SMSI = 0 nm**	**SMSI = 1 nm**	**SMSI = 2 nm**
2	17.82	97.95	104.98	36,32	141,22	140,73
3	21.95	99.61	120.30	41,11	147,36	168,37
4	24.12	93.95	124.95	43,25	135,30	174,52
5	24.96	87.71	123.63	46,46	126,96	169,41
6	25.57	80.84	117.22	49,77	116,91	162,12
7	25.78	75.51	111.31	48,79	110,79	157,14
8	25.95	70.14	102.99	45,45	100,36	145,04
9	26.16	66.21	97.00	32,65	96,65	136,90
10	26.35	63.89	93.38	28,76	92,14	133,06

Evaluation of the heat generated by Au SPR excitation

Irradiation at the SPR of Au can induce a temperature increase at the surface of the metal NPs, due to strong light absorption; this can even lead to a temperature increase extended to the whole sample supporting the NPs. With continuous LED excitation, energy is uniformly absorbed over time and the temperature increase at the NPs surface can be evaluated considering the heat transfer across the surface of a sphere when a source of constant heat is acting[1,2]

$$\Delta T = \frac{q_{NP}}{4\pi k_0 R_{NP}}$$

where q_{NP} is the heat generation rate, k_0 is the thermal conductivity of the matrix around the NP and R_{NP} is the NP radius.

To evaluate q_{NP} we started from the absorption cross section σ_{abs} of Au NPs multiplied by the incident LED fluence, I_0, and considered the borderline case – that is that all the absorbed power is converted into heat. Typical values of σ_{abs} for 5 nm Au NPs in water are in the 10^{-13}-10^{-14} cm^2 range.[3] During the experiment a continuous fluence of *ca.* 6 mW/cm^2 was provided, which gives a maximum absorbed power of 10^{-12} W per NP. With these values and considering the thermal conductivity of TiO_2 (5-12 $W\ K^{-1}\ m^{-1}$) a maximum temperature increase of 6.4 μK per NP is found.

This temperature increase at the surface of each Au NP is not sufficient to induce a relevant heating of TiO_2 and therefore no significant influence on the catalytic activity.

Our calculation is in agreement with the result reported by Govorov *et al*. who investigated Au NPs as potential heaters. For 10 nm NPs they found a sizable temperature variation only for fluences exceeding 10^3 W/cm^2.

References

(1) Govorov, A. O.; Zhang, W.; Skeini, T.; Richardson, H.; Lee, J.; Kotov, N. *Nanoscale Res. Lett.* **2006**, *1*, 84.

(2) Govorov, A. O.; Richardson, H. H. *Nano Today* **2007**, *2*, 30–38.

(3) Van Dijk, M.; Tchebotareva, L.; Orrit, M.; Lippitz, M.; Berciaud, S.; Lasne, D.; Cognet, L.; Lounis, B. *Phys. Chem. Chem. Phys.* **2006**, *8*, 3486.